Thy-1 Immunolabeled Thymocyte Microdomains Studied with the Atomic Force Microscope and the Electron Microscope

Jean Thimonier,*# Christine Montixi,# Jean-Paul Chauvin,*§ Hai Tao He,# José Rocca-Serra,*# and Jacques Barbet*#

*Centre National de la Recherche Scientifique GDR 976; #Centre d'Immunologie INSERM-CNRS de Marseille-Luminy (UMR 4); and §Laboratoire de Génétique et de Physiologie du Développement (CNRS-Université d'Aix-Marseille II UMR 9943), Parc Scientifique et Technologique de Luminy, Marseille, France

ABSTRACT The atomic force microscope (AFM) and the transmission electron microscope (TEM) have been used to study the morphology of isolated mouse thymocyte microdomains and Thy-1 antigen distribution at the surface of these structures. AFM images were recorded in air in the contact mode on membrane vesicles deposited on previously heated tissue culture plastic sheets and indirectly immunolabeled for Thy-1 expression with colloidal gold-conjugated secondary antibodies. AFM images of untreated plastic plates showed a very characteristic network of streaks 20–200 nm wide. Heating the plastic removed the streaks and provided flat surfaces (r.m.s. 1 nm). This substrate allowed strong adsorption and homogeneous spreading of the vesicles and easy manipulations during immunolabeling experiments. Vesicles flattened on the substrate without losing their morphology. The 10-nm membrane-bound gold beads were reproducibly imaged without degradation by repeated tip scanning. The observed microdomains had a mean diameter of 184 ± 76 nm, and 65% of them were specifically labeled. Images obtained with the TEM on the same vesicles, deposited on carbon-coated grids and negatively stained, confirmed the AFM observations. The size distribution of the microdomains was quite similar, but the number of beads per vesicle was significantly higher, and 76% of the vesicles were labeled. The difference may be explained 1) by removal of beads from the vesicles in the additional washing step with water, which was necessary for the AFM; 2) by tip-sample convolution; and 3) by statistical fluctuations.

INTRODUCTION

Adhesion and activation processes are governed by a wide range of molecular interactions that induce specific signals. The immunoglobulin superfamily (Hood et al., 1985) contains a large number of cellular membrane glycoproteins involved in specific recognition processes, cellular adhesion, or antigen presentation. Structural data on their tridimensional organization within cell membranes, either alone or as specific complexes, are key to current biology. Thy-1 is a heavily glycosylated (30%) protein composed of one immunoglobulin-like domain (Campbell et al., 1979) and is mainly expressed in thymus and neural tissues in rodents. The exact function of the Thy-1 molecule is not entirely clear, but Thy-1 is associated with other signal transduction molecules at the T-cell membrane (Stefanova et al., 1991) inside specialized membrane structures called *microdomains*. These structures are enriched in glycosphingolipids, cholesterol, and proteins containing a glycosylphosphatidyl inositol tail and can be biochemically isolated (Brown and Rose, 1992) as membrane vesicles.

The atomic force microscope (Binnig et al., 1986) belongs to the scanning probe microscope family. Its principle is based on the deformation of a cantilever scanning a sample, thus providing real-space information on its surface topography with high resolution. In biology (for reviews see Shao and Yang, 1995, and Shaper and Jovin, 1996), many results have been reported, including images of living cells (Henderson et al., 1992; Le Grimellec et al., 1994; Haydon et al., 1996), chromosomes (Rasch et al., 1993), or smaller structures such as lipids (Muscatello et al., 1996), DNA (Bezanilla et al., 1994; Mou et al., 1995a; Wyman et al., 1995; Hansma et al., 1996), or proteins, either isolated (Yang et al., 1994; Thimonier et al., 1995) or within bidimensional crystals (Hoh et al., 1993; Mou et al., 1995b; Müller et al., 1995). Direct observation of membrane proteins in their natural environment remains a challenge because topographical identification among a wide range of molecules is almost impossible, but AFM imaging combined with immunogold labeling allows the detection of cellular surface proteins with high specificity (Putman et al., 1993; Müller et al., 1996).

Therefore, to understand the distribution of Thy-1 in microdomains at the surface of mouse thymocytes, we performed an immunogold labeling study of membrane vesicles isolated from these cells, using the AFM and the TEM, and evaluated the respective advantages of these techniques in this context.

Received for publication 23 January 1997 and in final form 28 May 1997.

Address reprint requests to Dr. Jean Thimonier, CNRS GDR 976, Parc Scientifique et Technologique de Luminy, Case 901, 13288 Marseille Cedex 9, France. Tel.: 33-04-91829302; Fax: 33-04-91829320; E-mail: rocca@ciml.univ-mrs.fr.

0006-3495/97/09/1627/06 $2.00

MATERIALS AND METHODS

Microdomain isolation and substrate preparation

Thymocytes (5×10^8 to 1×10^9) were freshly isolated (Kruisbeek, 1994) from the thymus of 4–6-week-old NMRI mice (purchased from the Centre d'Elevage R. Janvier and maintained in the animal care facility at the CIML). Analysis by flow cytometry showed that more than 95% of the

cells were viable Thy-1-positive leukocytes. They were resuspended in 1 ml of buffer (25 mM Tris, pH 8, 150 mM NaCl, 5 mM EDTA) supplemented with a mixture of protease inhibitors (leupeptin 1 μg/ml, pepstatin 1 μg/ml, chymostatin 2 μg/ml) at 4°C. Cells were broken by gentle sonication at 4°C (five 5-s bursts; Vibracell, Bioblock Scientific). After centrifugation in a microfuge at 3000 rpm at 4°C for 10 min, the postnuclear supernatant was collected and then incubated with Brij 58 at a final concentration of 1%, for 1 h at 4°C. The lysate was then adjusted to 1.33 M sucrose by the addition of 2 ml of 2 M sucrose prepared in lysis buffer and placed at the bottom of an ultracentrifuge tube. A step sucrose gradient (0.2 M to 0.9 M) made up in lysis buffer without detergent was formed above this and centrifuged at 38,000 rpm for 15 h in an SW41 rotor (Beckman Instrument) at 4°C. Fractions (1 ml each) were harvested from the top. Glycosphingolipid microdomains migrate mainly in the low-density fractions 2, 3, and 4 (unpublished data), which were pooled before labeling experiments.

Modified plastic substrates for AFM were prepared by placing the external face of a Multiwell tissue culture plate (Falcon 3047; Becton Dickinson) over the flame of a Bunsen burner for 5 s.

Atomic force microscopy

AFM imaging was performed in air in the contact mode with a laboratory-built microscope (Perrot et al., 1994) using commercially available silicon nitride triangular microlevers (Park Scientific Instruments, Sunnyvale, CA) with an integrated pyramidal tip and a typical spring constant of 0.05 N/m.

Immunogold labeling procedures

For AFM observations, the heat-modified plastic plates were submitted to glow discharge (10 min) in an Edwards apparatus. Then, freshly isolated membrane vesicles were deposited on the plastic, left for 30 min at 4°C, and further incubated for 1 h at 4°C with phosphate-buffered saline (PBS) containing 0.1% bovine serum albumin (BSA). For immunolabeling, the samples were incubated for 30 min at 4°C with a rat monoclonal $IgG_{\gamma 2a,\kappa}$ anti-Thy-1 antibody (H194-92; Naquet et al., 1989) purified from ascites fluid and diluted to 15 μg/ml in PBS/0.1% BSA. Negative control was made with an irrelevant rat antibody (RB6–8C5; $IgG_{\gamma 2b,\kappa}$) at the same dilution. After they were washed in PBS, vesicles were incubated for 30 min at 4°C with 10-nm colloidal gold-labeled goat anti-rat IgG antibody (Biocell Research Laboratories, Cardiff, Wales) diluted to 1:20 in PBS/0.1% BSA. After they were washed in PBS, the samples were finally rinsed with distilled water and dried at room temperature.

For TEM studies, membrane vesicles were deposited for 3 min at 4°C on glow-discharged carbon-coated grids (Baltec, Balzers, Liechtenstein). Immunolabeling was performed using the same protocol as for AFM samples, except that incubation times with BSA and antibodies were reduced to 15 min, which gave the best labeling results. Final washing with distilled water was not carried out. Instead, the samples were stained for 1 min with uranyl acetate diluted to 1% in distilled water, and electron microscopy observations were performed with a Zeiss EM 912 microscope (Oberkochen, Germany).

RESULTS

Plastic substrate characterization

Untreated plastic tissue culture sheets (Fig. 1 *a*) presented typical features that consisted of a network of randomly oriented streaks. The lateral dimension of the structures (measured at half-height) was 75.5 ± 34.6 nm, and their height was 8.2 nm ± 3.8 nm. After heating, these features disappeared (Fig. 1 *b*) and gave way to a surface topography characterized by long-range undulations and reduced roughness (r.m.s. 1 nm). On a smaller scale on the order of microns, the r.m.s. value falls to 0.5 nm.

AFM observation of unlabeled microdomains

AFM images of membrane vesicles (Fig. 2) showed flat structures that kept their circular shape after deposition on the substrate. The larger vesicles appeared to have lost their central part, and only their contours remained visible, with a mean thickness of 3.5 ± 1.5 nm, which is smaller than the expected value for a biological membrane containing proteins. This difference was attributed to both dehydration and tip compression. Higher resolution AFM images of the top of intact vesicles (data not shown) did not give any information about a particular structural arrangement of the proteins in the membrane.

AFM and TEM studies of immunolabeled Thy-1 microdomains

After immunolabeling, vesicles remained visible, and individual membrane-bound gold beads were reproducibly imaged with the AFM. Gold bead sizes were measured in

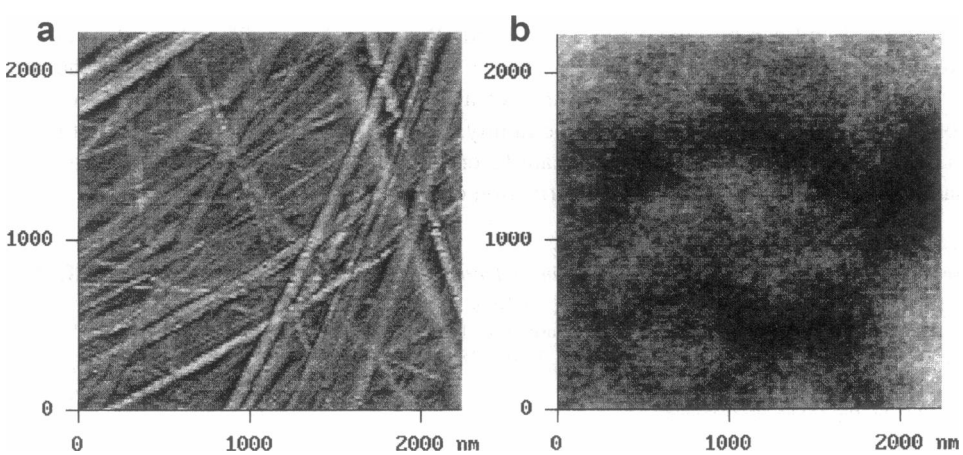

FIGURE 1 Atomic force microscopy images in air of tissue culture plates. (*a*) The surface of untreated plastic exhibits individual randomly oriented polystyrene streaks. (*b*) These characteristic structures are completely removed after heating the plate to provide a substrate presenting flat undulations. Images were displayed as top views after mean plane subtraction, and topography was coded with a 256 grey scale, from black (*bottom*) to white (*top*), corresponding to 2 nm and 5 nm full scale, respectively.

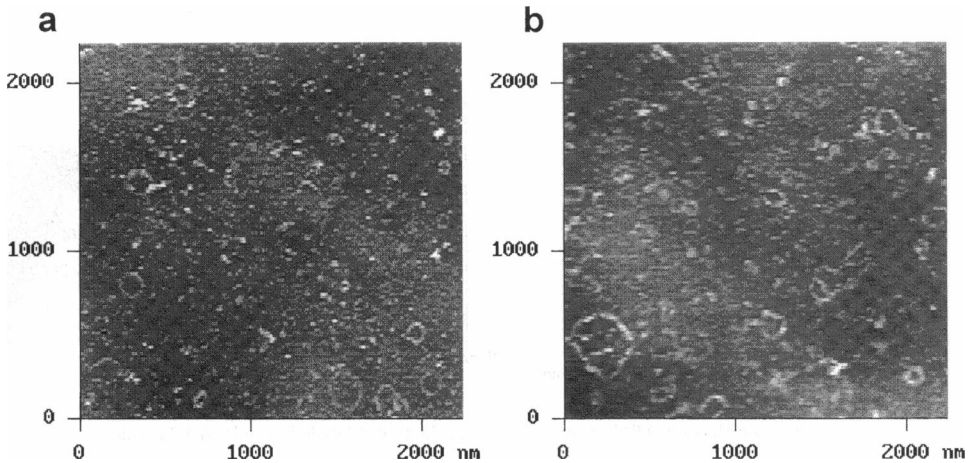

FIGURE 2 Atomic force microscopy images of air-dried mouse thymocyte membrane vesicles. Freshly prepared membrane vesicles were deposited on a modified plastic substrate, left for 30 min at 4°C, washed with phosphate saline buffer, and then again with distilled water. Vesicles flatten on the support and retain their circular shape. Most of the structures seem to have lost their central part, and only their contours remain visible. Images displayed in *a* and *b* correspond to close-up views of two different regions of the observed sample.

different experiments with different tips (Fig. 3 and 4). Mean values of their height and lateral width measured at half-height, 8.9 nm ± 1.4 nm and 29 nm ± 8 nm, respectively, were in good agreement with the 9.9-nm diameter given by the manufacturer. The increased lateral size of the beads was attributed both to the presence of the bound antibodies, which are not detected in TEM images, and to the broadening effect due to the well-known tip-sample convolution observed in scanning probe microscopy experiments (Barbet et al., 1993; Keller and Franke, 1993; Xu and Arnsdorf, 1994). Thus, bead imaging afforded an internal control of resolution during scanning (Vesenka et al., 1993).

In the AFM immunolabeling experiments, the labeled vesicles represented 65% of the total population, with a mean diameter of 184 ± 76 nm. The vesicles that did not bind the gold beads had a diameter of 158 ± 26 nm. TEM experiments (Fig. 5) showed that 76% of the vesicles were labeled, with a mean diameter of 149 ± 62 nm. Unlabeled vesicles were also characterized by lower dimensions (117 ± 34 nm). Smaller vesicles bound a lower number of gold beads. To further study the relationship between size and labeling, we arbitrarily defined three size classes and determined the mean number of membrane-bound gold beads for each class (Table 1). AFM data showed that the most represented subpopulation of labeled vesicles (72%) corresponded to the 150–300-nm class, whereas for unlabeled vesicles, the 0–150-nm class (50%) was the most represented. From TEM observation we again deduced that the majority of labeled (86%) and unlabeled (30%) membranes are found in the 150–300-nm and 0–150-nm classes, respectively.

Table 1 also shows that the mean number of beads per labeled vesicle found in AFM experiments is low. This mean number, calculated over the whole population of vesicles, is less than 2. Thus, according to the Poisson distribution, statistical fluctuations can account for at least 12% of unlabeled vesicles. By contrast, in TEM experiments, the mean number of beads per vesicle is larger, and statistical fluctuations are bound to be much lower (0.3%). This reconciles the two figures for the proportion of labeled vesicles: 76% for TEM and 65% plus ~12% of apparently unlabeled vesicles for AFM.

In a series of AFM and TEM control experiments, performed with irrelevant primary antibody (data not shown), less than 6% of the vesicles were labeled. Otherwise the size and morphology of the vesicles were quite comparable.

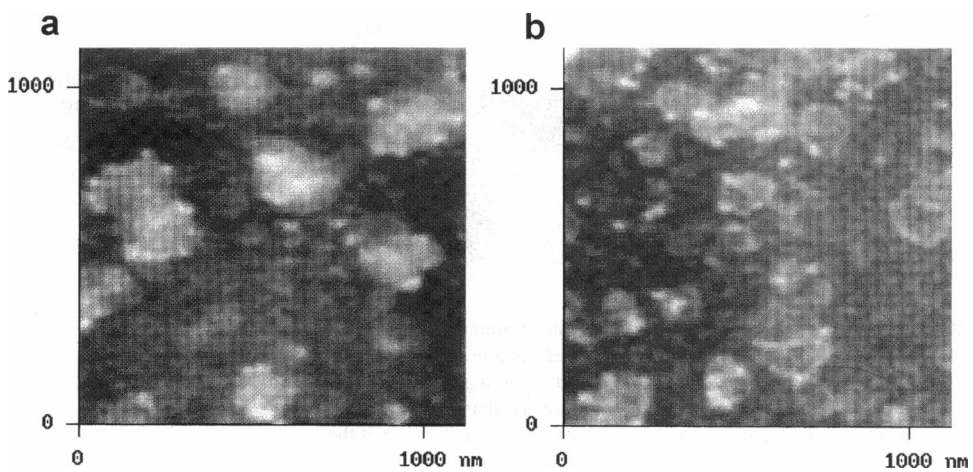

FIGURE 3 AFM images (*a* and *b*) of immunogold-labeled membrane vesicles adsorbed on a heated plastic substrate. Labeling was performed with a primary rat anti-Thy-1 antibody and colloidal gold-conjugated secondary antibodies (see Materials and Methods). Individual 10-nm membrane-bound gold beads are mainly observed in the periphery of the structures.

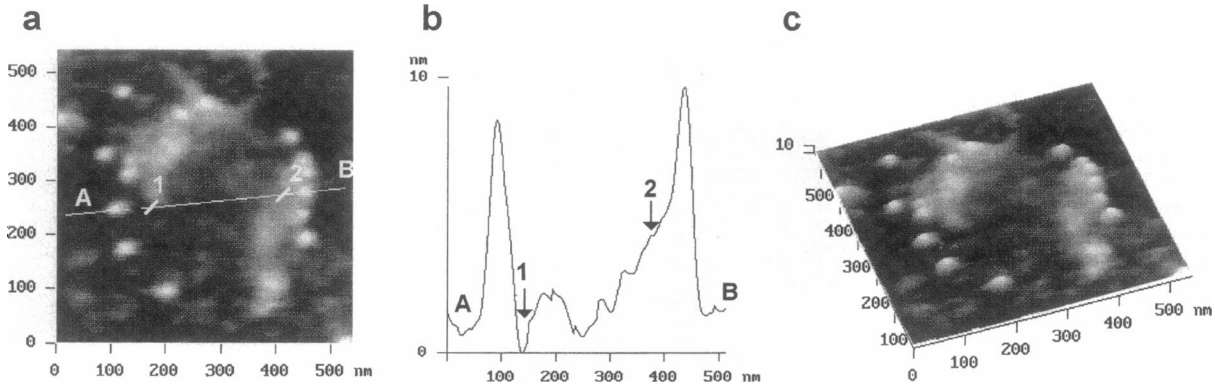

FIGURE 4 Higher magnification AFM image of an individual gold-labeled vesicle. (*a*) Two-dimensional representation and (*b*) cross-section analysis corresponding to the line *A–B* drawn in *a*. Vertical dimensions of the membrane-bound gold beads localized on the left and right sides of the vesicle are 10.5 nm and 9.8 nm, respectively, and the membrane thickness measured between level 1 (bare substrate) and level 2 (top of the membrane) is 3 nm. (*c*) Pseudo-three-dimensional representation of the same vesicle corresponding to *a*, with a 20° rotation in the plane and a 45° tilt.

DISCUSSION

To improve specific adsorption and homogeneous distribution of biological samples on the usual scanning probe microscopy substrates (graphite, silicon, glass, mica, or gold), chemical modifications of the substrate and the samples to be analyzed have been tested (Ill et al., 1993; Karrasch et al., 1993; Mazeran et al., 1995; Rekesh et al., 1996; Wagner et al., 1996). In the case of either natural or synthetic membrane structures, AFM observations did not necessarily require such modifications. However, based on our personal experience, the poor reproducibility of the results obtained with graphite or mica led us to look for another substrate. We tested common tissue culture plastic plates and found that spreading and adhesion of the biological membranes were homogeneous and strong enough to allow reproducible AFM imaging. Moreover, labeling experiments performed directly in the wells were easier. Imaging of membrane vesicles deposited on untreated plastic plates was possible (data not shown). However, streaks were present on the untreated substrate, which may be confusing for imaging. We assumed that they were made during the molding step of the plate. After heating, the polystyrene streaks disappeared. The local 0.5 r.m.s. roughness observed, although quite high as compared to mica (0.06 nm) or silicon (0.15 nm), is not a problem for vesicle observation. Even if this method remains empirical, inasmuch as we did not control the temperature to which the plastic was heated, we have been able to easily prepare useful AFM substrates with high reproducibility. So we decided to use them to avoid the membrane deformations caused by the underlying structures.

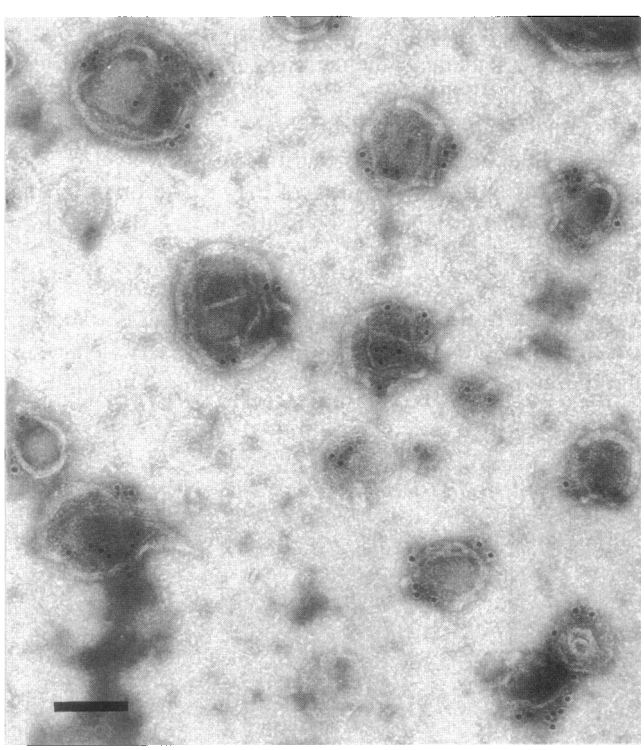

FIGURE 5 Transmission electron micrograph of immunogold-labeled thymocyte membrane vesicles. Freshly prepared microdomains were deposited on glow discharge carbon grids, labeled according to the protocol described in Materials and Methods and negatively stained with uranyl acetate. Colloidal gold markers are localized both around and on top of the vesicles. The scale bar represents 120 nm.

TABLE 1 Comparative AFM and TEM distributions of specific gold labeling

Technique	Vesicle diameter (nm)	Observed vesicles (%)	Labeled vesicles (% of total)	Labeled vesicles (% of class)	Mean number of bound gold beads*
AFM	0–150	40	20	50	1.6
	150–300	54	39	72	2.5
	>300	6	6	100	7.1
	Overall	100	65	65	2.6
TEM	0–150	67	47	70	3.7
	150–300	30	26	86	10.7
	>300	3	3	100	22.5
	Overall	100	76	76	6.7

*Calculated over all labeled vesicles.

To understand the potential role of membrane glycosphingolipid domains in signal transduction mechanisms and the biological development of mouse thymocytes, a precise morphological characterization of thymocyte-isolated microdomains and Thy-1 distribution analysis on their surface is necessary. Because direct AFM visualization of Thy-1 molecules on the surface of these structures was not possible, we used indirect immunogold labeling of this antigen. The proportion of specifically labeled membrane vesicles and labeling efficiency analyzed for each size class of microdomains in AFM images are lower than the values obtained from TEM observations. This difference may be explained 1) by the fact that only clearly individualized beads were counted with the AFM, larger structures being counted only once, although they may correspond to aggregates of a few beads masked by tip-sample convolution; and 2) by the loss of material in the inner part of some vesicles during the AFM sample preparation. The hypothesis that beads were swept away by the scanning tip was excluded because there was no trace of tip jumps or strikes in the images (Barbet et al., 1993), and the images appeared unchanged on repeated scanning. To avoid formation of salt crystals after drying, AFM samples were finally rinsed with distilled water, which we suspect partly destroys or removes some membrane material. There is a possibility that low osmolarity had swollen and transformed the central part of the vesicles in fragments. This effect can also explain the apparently higher background of beads apparently located outside vesicles in the AFM images (Figs. 3, 4, and 5). If this was the case, to improve quantitative labeling, AFM observations should be performed directly under physiological buffer, just after immunolabeling (Müller et al., 1996). As a result of these effects, the mean number of gold beads per labeled vesicles in AFM images is low, and statistical fluctuations can account for ~12% of unlabeled Thy-1-positive vesicles. Thus, when this correction factor is used for AFM measurements, both TEM and AFM demonstrate the presence of ~25% of Thy-1-negative vesicles. The origin of this population of vesicles is not clear. Studies are in progress to determine whether these vesicles are contaminant in the preparation, originating from other cells or other cell membrane compartments, Thy-1-negative microdomains, or both. In any case, the number of Thy-1-negative cells in the original cell population is too small to explain this observation by itself.

CONCLUSION

Atomic force microscopy was applied to characterize Thy-1-containing plasma membrane microdomains purified from mouse thymocytes by using Thy-1-specific immunolabeling. The use of modified common tissue culture plastic plates as an AFM substrate allowed reproducible imaging of specific membrane-bound colloidal gold labels, and statistical analysis showed that Thy-1 is localized in morphologically well-defined structures. TEM afforded comparable results concerning the size distribution of the membrane vesicles, and both techniques demonstrated that the sucrose gradient purification technique affords a reasonably homogeneous population of vesicles, of which 75% are Thy-1-positive.

We expect that further studies directly performed on immunogold-labeled thymocytes instead of membrane preparations (either in air or in liquid) will afford an unambiguous answer concerning the natural distribution of Thy-1 on the surface of these cells.

REFERENCES

Barbet, J., A. Garvin, J. Thimonier, J.-P. Chauvin, and J. Rocca-Serra. 1993. Scanning tunneling microscopy of colloidal gold beads. *Ultramicroscopy.* 50:355–363.

Bezanilla, M., B. Drake, E. Nudler, M. Kashlev, P. K. Hansma, and H. G. Hansma. 1994. Motion and enzymatic degradation of DNA in the atomic force microscope. *Biophys. J.* 67:2454–2459.

Binnig, G., C. F. Quate, and Ch. Gerber. 1986. Atomic force microscope. *Phys. Rev. Lett.* 56:930–933.

Brown, D. A., and J. K. Rose. 1992. Sorting of GPI-anchored proteins to glycolipid-enriched membranes subdomains during transport to the apical cell surface. *Cell.* 68:533–544.

Campbell, D. G., A. F. Williams, P. M. Barclay, and K. B. M. Reid. 1979. Structural similarities between Thy-1 antigen from rat brain and immunoglobulin. *Nature.* 282:341–342.

Hansma, H. G., I. Revenko, K. Kim, and D. E. Laney. 1996. Atomic force microscopy of long and short double-stranded, single-stranded and triple-stranded nucleic acids. *Nucleic Acids Res.* 24:713–720.

Haydon, P. G., R. Lartius, V. Parpura, and S. P. Marchese-Ragona. 1996. Membrane deformation of living glial cells using atomic force microscopy. *J. Microsc.* 182:14–120.

Henderson, E., P. G. Haydon, and D. S. Sakaguchi. 1992. Actin filament dynamics in living glial cells imaged by atomic force microscopy. *Science.* 257:1944–1946.

Hoh, J. H., G. Sosinsky, J. P. Revel, and P. K. Hansma. 1993. Structure of the extracellular surface of the gap junction by atomic force microscopy. *Biophys. J.* 65:149–163.

Hood, L., M. Kronenberg, and T. Hunkapiller. 1985. T cell antigen receptors and the immunoglobulin supergene family. *Cell.* 40:225–229.

Ill, C. R., V. M. Keivens, J. E. Hale, K. K. Nakamura, R. A. Jue, Cheng S., E. D. Melcher, B. Drake, and M. C. Smith. 1993. A COOH-terminal peptide confers regiospecific orientation and facilitates atomic force microscopy. *Biophys. J.* 64:919–924.

Karrasch, S., M. Dolder, F. Schabert, J. Ramsden, and A. Engel. 1993. Covalent binding of biological samples to solid supports for scanning probe microscopy in buffer solution. *Biophys. J.* 65:2437–2446.

Keller, D. J., and F. S. Franke. 1993. Envelope reconstruction of probe microscope images. *Surface Sci.* 294:409–419.

Kruisbeek, A. D. 1994. Isolation of mouse mononuclear cells. *In* Current Protocols in Immunology, Vol. 1, unit 3.1. J. E. Coligan, A. M. Kruisbeek, D. H. Margulies, E. M. Shevach, and W. Strober, editors. Green Publishing Associates Inc. and John Wiley and Sons Inc.

Le Grimellec, C., E. Liesniewska, C. Cachia, J. P. Schreiber, F. de Fornel, and J. P. Goudonnet. 1994. Imaging of the membrane surface of MDCK cells by atomic force microscopy. *Biophys. J.* 67:36–41.

Mazeran, P.-E., J.-L. Loubet, C. Martelet, and A. Theretz. 1995. Under buffer SFM observation of immunospecies adsorbed on a cyano grafted silicon substrate. *Ultramicroscopy.* 60:33–40.

Mou, J., D. M. Czajkowsky, Y. Zhang, and Z. Shao. 1995a. High-resolution atomic-force microscopy of DNA: the pitch of the double helix. *FEBS Lett.* 371:279–282.

Mou, J., J. Yang, and Z. Shao. 1995b. Atomic force microscopy of cholera toxin B-oligomers bound to bilayers of biologically relevant lipids. *J. Mol. Biol.* 248:507–512.

Müller, D. J., F. A. Schabert, G. Büldt, and A. Engel. 1995. Imaging purple membranes in aqueous solutions at sub-nanometer resolution by atomic force microscopy. *Biophys. J.* 68:1681–1686.

Müller, D. J., C.-A. Schoenenberger., G. Büldt, and A. Engel. 1996. Immuno-atomic force microscopy of purple membrane. *Biophys. J.* 70:1796–1802.

Muscatello, U., G. Valdre, and U. Valdre. 1996. Atomic force microscopy observations of acyl chains in phospholipids. *J. Microsc.* 182:200–207.

Naquet, P., J. Barbet, S. Pont, S. Marchetto, M. Barad, C. Devaux, G. Rougon, and M. Pierres. 1989. Characterization of Thy-1 with monoclonal antibodies and evidence of Thy-3. *In* Cell Surface Antigen Thy-1. A. E. Reif and M. Schlesinger, editors. Marcel Dekker, New York and Basel. 99–117.

Perrot, E., M. Dayez, A. Humbert, O. Marti, C. Chapon, and C. R. Henry. 1994. Atomic-scale resolution on the MgO(100) surface by scanning force and friction microscopy. *Europhys. Lett.* 26:659–663.

Putman, C. A. J., B. G. de Grooth, P. K. Hansma, N. K. van Hulst, and J. Greve. 1993. Immunogold labels: cell-surface markers in atomic force microscopy. *Ultramicroscopy.* 48:177–182.

Rasch, P., U. Wiedemann, J. Wienberg, and W. M. Heckl. 1993. Analysis of banded human chromosomes and in situ hybridization patterns by scanning force microscopy. *Proc. Natl. Acad. Sci. USA.* 90:2509–2511.

Rekesh, D., Y. Lyubchenko, L. S. Shlyakhtenko, and S. M. Lindsay. 1996. Scanning tunneling microscopy of mercapto-hexyl-oligonucleotides attached to gold. *Biophys. J.* 71:1079–1086.

Shao, Z., and J. Yang. 1995. Progress in high resolution atomic force microscopy in biology. *Q. Rev. Biophys.* 28:195–251.

Shaper, A., and T. Jovin. 1996. Striving for atomic resolution in biomolecular topography: the scanning force microscope. *BioEssays.* 18: 925–935.

Stefanova, I., V. Horejsi, I. J. Ansotegui, W. Knapp, and H. Stockinger. 1991. GPI-anchored cell-surface molecules complexed to protein tyrosine kinases. *Science.* 254:1016–1019.

Thimonier, J., J.-P. Chauvin, J. Barbet, and J. Rocca-Serra. 1995. Preliminary studies of an immunoglobulin M by near-field microscopies. *J. Trace Microprobe Tech.* 13:353–359.

Vesenka, J., S. Manne, R. Giberson, T. Marsh, and E. Henderson. 1993. Colloidal gold particles as an incompressible atomic force microscope imaging standard for assessing the compressibility of biomolecules. *Biophys. J.* 65:992–997.

Wagner, P., M. Hegner, P. Kernen, F. Zaugg, and G. Semenza. 1996. Covalent immobilization of native biomolecules onto Au(111) via *N*-hydroxysuccinimide ester functionalized self-assembled monolayers for scanning probe microscopy. *Biophys. J.* 70:2052–2066.

Wyman, C., E. Grotkopp, C. Bustamante, and H. C. M. Nelson. 1995. Determination of heat-shock transcription factor 2 stoechiometry at looped DNA complexes using scanning force microscopy. *EMBO J.* 14:117–123.

Xu, S., and M. F. Arnsdorf. 1994. Calibration of the scanning (atomic) force microscope with gold particles. *J. Microsc.* 173:199–210.

Yang, J., J. Mou, and Z. Shao. 1994. Molecular resolution atomic force microscopy of soluble proteins in solution. *Biochim. Biophys. Acta.* 1199:105–114.